

Sowers, *Science* **242**, 1675 (1988)]. It ceases to rise near the base of the firm when dense layers begin to close off, preventing further diffusion. At Taylor Dome,  $\delta^{15}\text{N}$  values typical of Holocene ice [ $-0.25$  per mil (‰)] are reached at a firm density of  $800\text{ kg m}^{-3}$  [C. M. Sucher, thesis, University of Rhode Island, Narragansett (1997)]. This value is about 2% lower than that obtained at GISP2 or the South Pole [M. Battle *et al.*, *Nature* **383**, 231 (1996)].

12. T. Sowers, M. Bender, D. Raynaud, Y. S. Korotkevich, *J. Geophys. Res.* **97**, 15683 (1992).

13. The original firm thickness is assumed to be 50 m (ice equivalent depth). Thinning due to glacier flow was calculated as described [E. D. Waddington, D. L. Morse, P. M. Grootes, E. J. Steig, *NATO ASI Ser.* **112**, 499 (1993); D. L. Morse, thesis, University of Washington, Seattle (1997)].

14. The equation  $\alpha = 4\text{‰}^{\circ}\text{C}^{-1}$  (equivalent to  $0.5\text{‰}^{\circ}\text{C}^{-1}$  for  $\delta^{18}\text{O}$ ) agrees with borehole temperature analyses at Taylor Dome showing a  $\sim 1.5^{\circ}$  cooling at Taylor Dome since about 4 kyr B.P., during which  $\delta\text{D}$  dropped by  $\sim 6\text{‰}$  [E. D. Waddington and G. D. Clow, *Eos Trans.* **78**, F41 (1997)]. Varying  $\alpha$  by  $\pm 1.5\text{‰}^{\circ}\text{C}^{-1}$  simulates possible temporal changes [K. M. Cuffey *et al.*, *Science* **270**, 455 (1995)].

15.  $b$  at depth  $z$  is given by  $F_{\text{dry}}/([\text{Be}]_z - [\text{Be}]_{\text{wet}})$ , where  $[\text{Be}]_{\text{wet}} = 5 \pm 5$  atoms  $\text{mg}^{-1}$  (6) is the concentration of  $^{10}\text{Be}$  in wet precipitation, and  $F_{\text{dry}} = b(0)([\text{Be}]_0 - [\text{Be}]_{\text{wet}})$  is the dry-deposition flux.

16. E. J. Steig, P. J. Polissar, M. Stuver, *Antarct. J. U. S.* **30**, 95 (1995); G. M. Raisbeck and F. Yiou, *Ann. Glaciol.* **7**, 138 (1985).

17. E. J. Steig, P. J. Polissar, M. Stuver, R. C. Finkel, P. M. Grootes, *Geophys. Res. Lett.* **23**, 523 (1996); E. Bard, G. M. Raisbeck, F. Yiou, J. Jouzel, *Earth Planet. Sci. Lett.* **150**, 453 (1997); R. C. Finkel and K. Nishiizumi, *J. Geophys. Res.* **102**, 26699 (1997).

18. R. B. Alley *et al.*, *J. Glaciol.* **41**, 503 (1995). In the Taylor Dome core, the correlation coefficient between  $^{10}\text{Be}$  and  $\text{SO}_4$  is  $>0.75$ .

19. E. J. Steig, D. L. Morse, E. D. Waddington, P. J. Polissar, *Geophys. Res. Lett.* **25**, 163 (1998).

20. G. de Q. Robin, *Philos. Trans. R. Soc. London Ser. A* **280**, 143 (1977); J. Jouzel *et al.*, *Quat. Res.* **31**, 135 (1989).

21. E. D. Waddington and D. L. Morse, *Ann. Glaciol.* **20**, 219 (1994); E. J. Steig, *ibid.* **25**, 418 (1997).

22. The uncertainty in GISP2  $\Delta$ age is taken from comparison of results from two independent calculations, which are in agreement within  $\pm 100$  years [(8) and J. Schwander *et al.*, *J. Geophys. Res.* **102**, 19483 (1997)]. Uncertainty in the curve match is taken as one-half the sampling interval, generally 1000 years for the period from 20 to 15 kyr B.P. and 150 years for the period from 15 to 10 kyr B.P.

23. S. J. Lehman and L. D. Keigwin, *Nature* **356**, 757 (1992); *ibid.* **358**, 197 (1992).

24. T. J. Crowley, *Paleoceanography* **7**, 489 (1992); T. Stocker, *ibid.*, p. 529; W. S. Broecker, *Science* **278**, 1582 (1997).

25. T. J. Crowley and C. L. Parkinson, *Clim. Dyn.* **3** (1988); W. S. Broecker and G. H. Denton, *Geochim. Cosmochim. Acta* **53**, 2465 (1989); J. Imbrie *et al.*, *Paleoceanography* **7**, 701 (1993). Compatible with this explanation,  $\delta^{13}\text{C}$  ratios in benthic foraminifera from deep-sea sediment cores indicate that the flux of NADW to the Southern Ocean increased abruptly at 14 to 15 kyr B.P. Moreover, the subdued nature of the B/A-YD oscillation at Taylor Dome, relative to that in the central Greenland records, parallels the relatively small benthic  $\delta^{13}\text{C}$  response during this period [C. D. Charles and R. G. Fairbanks, *Nature* **355**, 416 (1992); C. D. Charles, J. Lynch-Stieglitz, U. S. Ninnemann, R. G. Fairbanks, *Earth Planet. Sci. Lett.* **142**, 19 (1996)].

26. S. S. Jacobs, R. G. Fairbanks, and Y. Horibe [*Antarct. Res. Ser.* **43**, 203 (1985)] estimate that southward oceanic heat transport provides a net flux of heat to the atmosphere of  $\sim 3\text{ W/m}^2$  along the Antarctic coastal margin. Local heat fluxes from leads and polynyas in the western Ross Sea, kept open by the strong westerly katabatic wind flow [D. D. Kurtz and D. Bromwich, *ibid.*, p. 177; H. J. Zwally and J. C. Comiso, *ibid.*, p. 203], may be two orders of magnitude higher [D. J. Cavalieri and S. Martin, *ibid.*, p. 227].

27. U. Mikolajewicz *et al.*, *Nature* **387**, 384 (1997); S. Manabe and R. J. Stouffer, *Paleoceanography* **12**, 321 (1997).

28. A. Schiller, U. Mikolajewicz, R. Voss, *Max-Planck-Inst. Meteorol. Rep.* **188** (1996); *Clim. Dyn.* **13**, 325 (1997).

29. The sensitivity of Taylor Dome to local oceanographic conditions may depend on ice sheet configuration, especially the position of the Ross Ice Sheet/Ice Shelf margin. Although the Ross Ice Sheet may not have reached all the way to the continental shelf break during the last glacial maximum [K. J. Licht, A. E. Jennings, J. T. Andrews, K. M. Williams, *Geology* **24**, 223 (1996)], the distance between Taylor Dome and seasonally open water would have been greater, and

local atmospheric circulation patterns may have been altered [D. L. Morse, E. D. Waddington, E. J. Steig, *Geophys. Res. Lett.* **25**, 3383 (1998)]. We do not therefore expect a simple linear relation between proxies of ocean circulation and Taylor Dome  $\delta\text{D}$  even if, as we suggest, changes in ocean circulation are the primary forcing mechanism.

30. We thank G. Denton and M. Stuver for suggesting an ice core at Taylor Dome, P. Grootes for directing the field program, the Polar Ice Coring Office and Antarctic Program of NSF for logistical and financial support, and R. Alley and M. Kaplan for helpful comments on the manuscript.

15 July 1998; accepted 28 August 1998

## Solution Properties of Single-Walled Carbon Nanotubes

Jian Chen, Mark A. Hamon, Hui Hu, Yongsheng Chen, Apparao M. Rao, Peter C. Eklund, Robert C. Haddon\*

Naked metallic and semiconducting single-walled carbon nanotubes (SWNTs) were dissolved in organic solutions by derivatization with thionylchloride and octadecylamine. Both ionic (charge transfer) and covalent solution-phase chemistry with concomitant modulation of the SWNT band structure were demonstrated. Solution-phase near-infrared spectroscopy was used to study the effects of chemical modifications on the band gaps of the SWNTs. Reaction of soluble SWNTs with dichlorocarbene led to functionalization of the nanotube walls.

With novel structural, electronic, and mechanical properties, SWNTs constitute an important new form of carbon that may find applications in many fields (1). The functionalization chemistry of the open ends, the exterior walls (convex face), and the interior cavity (concave face) of the SWNTs is expected to play a vital role in tailoring the properties of these materials and the engineering of nanotube devices. However, all of the currently known forms of SWNT material are insoluble in organic solvents (2, 3), making it difficult to explore and understand the chemistry of SWNTs (4) at the molecular level. We report here an approach to the dissolution of shortened SWNTs (5) in common organic solvents. Various solution spectroscopies were applied to characterize the dissolved SWNTs. We found that the band gaps of some types of SWNTs can be measured directly by solution-phase near-infrared (IR) spectroscopy, which allows the study of the effects of chemical modifications on the band gaps of SWNTs, the key to the molecular design of new SWNT-based materials.

Solution-phase wall chemistry was demonstrated by reaction of the soluble SWNTs (s-SWNTs) with dichlorocarbene. The s-SWNTs will have a rich solution chemistry, perhaps rivaling that of the fullerenes. They are versatile precursors to nanotube-based copolymers, composites, and metal ligands.

The SWNT-containing raw soot (40 to 60% purity, obtained from CarboLex Inc.) was prepared by the modified electric-arc technique (3). Purified SWNTs (>90%) and shortened SWNTs (100 to 300 nm in length) were obtained by the method of Smalley and co-workers (5). In the final step of purification, we added HCl to the aqueous suspension of SWNTs before collecting the sample, so that the opened ends of the purified SWNTs were terminated with carboxylic acid groups ( $-\text{COOH}$ , IR frequency  $\nu_{\text{C=O}} = 1719\text{ cm}^{-1}$ ) rather than carboxylate groups ( $-\text{COO}^-$ ,  $\nu_{\text{C=O}} = 1620\text{ cm}^{-1}$ ) (Fig. 1). The shortened SWNTs have similar IR features. The Raman spectrum of the shortened SWNTs collected with 1064-nm excitation ( $\omega_r = 161\text{ cm}^{-1}$ ,  $\omega_t = 1595\text{ cm}^{-1}$ , where  $\omega_r$  and  $\omega_t$  are the Raman-active radial mode and tangential mode frequencies of SWNTs, respectively) is close to that of raw soot ( $\omega_r = 162\text{ cm}^{-1}$ ,  $\omega_t = 1592\text{ cm}^{-1}$ ). The Raman radial mode of the SWNTs is sensitive to the diameter  $d$  but not to the symmetry of the nanotube (6, 7); hence, if  $\omega_r\text{ (cm}^{-1}\text{)} = 223.75$

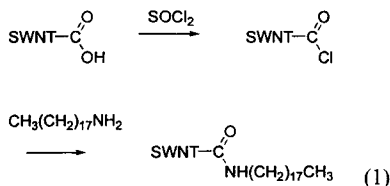
Departments of Chemistry and Physics, Center for Applied Energy Research and Advanced Carbon Materials Center, University of Kentucky, Lexington, KY 40506, USA.

\*To whom correspondence should be addressed. E-mail: haddon@pop.uky.edu

## REPORTS

( $\text{cm}^{-1} \text{ nm}$ )/ $d$  (nm) (7), the average diameter of the shortened SWNTs in our sample is estimated to be 1.38 nm.

To solubilize the SWNTs, we added the long-chain molecule octadecylamine (ODA) to the open ends of shortened SWNTs via formation of the amide functionality (5):



The s-SWNTs were prepared as follows: 100 mg of shortened SWNTs (5) were stirred in 20 ml of  $\text{SOCl}_2$  [containing 1 ml of dimethylformamide (DMF)] at  $70^\circ\text{C}$  for 24 hours. After centrifugation, the brown-colored supernatant was decanted and the remaining solid was washed with anhydrous tetrahydrofuran (THF). After centrifugation, the pale yellow-colored supernatant was decanted. The remaining solid was dried at room temperature under vacuum. A mixture of the resulting SWNTs and 2 g of ODA (melting point,  $55^\circ$  to  $57^\circ\text{C}$ ) was heated at  $90^\circ$  to  $100^\circ\text{C}$  for 96 hours. After cooling to room temperature, the excess ODA was removed by washing with ethanol four times (5 to 10 min sonication at 40 KHz). The remaining solid was dissolved in dichloromethane, and after filtration, the black-colored filtrate was taken to dryness on a rotary evaporator. The resulting black solid was dried at room temperature under vacuum. The yield of s-SWNTs is usually  $>60\%$  (based on shortened SWNTs).

Reaction of SWNT-COCl with excess ODA in toluene at room temperature for several days produced only trace amounts of s-SWNTs. The key to the high-yield preparation of s-SWNTs in our approach is the application of heat to the mixture of SWNT-COCl and ODA for an extended period of time. During this process, the volume of the SWNTs expands several times, perhaps be-

cause of exfoliation of the SWNTs bundles to give individual nanotubes.

In sharp contrast to the as-prepared shortened SWNTs, which are insoluble in organic solvents, the s-SWNTs have substantial solubility in chloroform, dichloromethane, aromatic solvents (benzene, toluene, chlorobenzene, 1,2-dichlorobenzene), and  $\text{CS}_2$ . The solubilities of s-SWNTs in 1,2-dichlorobenzene and  $\text{CS}_2$  are  $>1$  mg/ml. The black-colored (unsaturated) solution of s-SWNTs is visually nonscattering (Fig. 2) (very dilute solutions are brown), and no precipitation was observed upon prolonged standing. Like fullerenes, the s-SWNTs are insoluble in water, ethanol, and acetone. The IR spectrum of soluble SWNTs indicated the formation of the amide bond (Fig. 1):  $\nu_{\text{C=O}} = 1663 \text{ cm}^{-1}$  and  $1642 \text{ cm}^{-1}$ .

Proton nuclear magnetic resonance ( $^1\text{H}$  NMR, 200 MHz,  $\text{CDCl}_3$ ) of s-SWNTs showed the presence of the long aliphatic chain at the ends of the SWNTs:  $\delta$  0.88 (3H, t,  $\text{CH}_3$ ), 1.23 (32H, s,  $16 \times \text{CH}_2$ ). The  $\text{CH}_2$  group directly attached to the amide group at the ends of the SWNTs shows several broad signals in the range of  $\delta$  2.0 to 3.5; the integral of all of these signals corresponds to 2H, which suggests the existence of magnetically different types of SWNTs in our samples. There is prior support for the existence of large diamagnetic ring currents in carbon nanotubes (8, 9).

The Raman spectrum of the s-SWNTs in  $\text{CS}_2$  solution ( $\omega_r = 170 \text{ cm}^{-1}$ ,  $\omega_t = 1590 \text{ cm}^{-1}$ ; Fig. 3) is similar to that of shortened SWNTs ( $\omega_r = 161 \text{ cm}^{-1}$ ,  $\omega_t = 1595 \text{ cm}^{-1}$ ), but the radial mode frequency is upshifted  $9 \text{ cm}^{-1}$  and the tangential mode frequency is downshifted  $5 \text{ cm}^{-1}$ . The origin of this difference is not clear at present. If the upshift in the radial mode frequency reflects purely the difference of nanotube diameters, then the average diameter of s-SWNTs is estimated to be 1.31 nm. Doping also affects the radial and tangential mode frequencies of SWNTs (10).

The near = FTIR (Fourier transform IR) spectra of s-SWNTs in  $\text{CS}_2$  solution (Fig. 4)

showed the presence of three major signals:  $9791 \text{ cm}^{-1}$  (1.21 eV),  $9172 \text{ cm}^{-1}$  (1.14 eV), and  $5386 \text{ cm}^{-1}$  (0.67 eV). The signal at 0.67 eV is due to the band gap transition in semiconducting chiral nanotubes, which was previously observed by scanning tunneling microscopy (STM) (11, 12) and electron energy-loss spectroscopy (EELS) (13). The signal at 1.21 eV was also observed by EELS (13). Although the features at 1.21 and 1.14 eV correspond to the energy separation of the second pair of singularities in the density of states (DOS) of the semiconducting chiral SWNTs (11), these features are more likely to arise from metallic armchair nanotubes (6), because we found that the relative ratio of the 1.21/1.14 eV and 0.67 eV signals varies in batches of s-SWNTs originating from different sources of raw soot. If the 0.67 eV and 1.21/1.14 eV signals came from the energy separation of the first pair and second pair of singularities in semiconducting chiral SWNTs, then the ratio of 0.67 eV and 1.21/1.14 eV signals should be constant. In fact, our experimental data ( $d = 1.31$  to  $1.38$  nm, energy gap  $E_{\text{gap}} = 1.21$  eV,  $\omega_r = 170 \text{ cm}^{-1}$ ) are in good agreement with the calculated data for the metallic armchair (10,10) SWNT ( $d = 1.36$  nm,  $E_{\text{gap}} = 1.28$  eV,  $\omega_r = 165 \text{ cm}^{-1}$ ) (6), which suggests that an appreciable proportion of our sample is (10,10) SWNTs (2).

Doped SWNTs represent a new family of synthetic metals (10, 14, 15). Both bromine and iodine doping reduce the resistivity of SWNTs



Fig. 2. Unsaturated  $\text{CS}_2$  solution of s-SWNTs.

Fig. 1. FTIR spectra (Nicolet Magna-IR 560 ESP spectrometer) of purified SWNTs (top, KBr pellet), s-SWNTs [middle, SpectraTech Thunderdome attenuated total reflectance sample stage (ATR)], and ODA (bottom, ATR), with baseline correction.

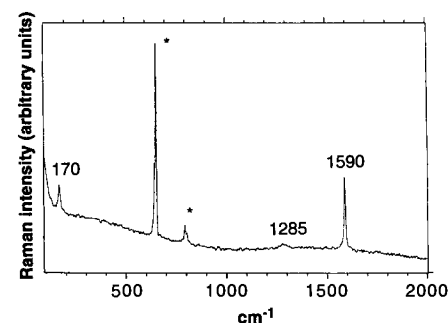
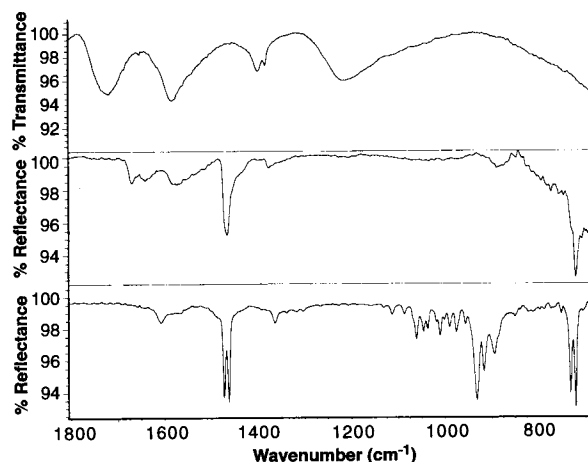


Fig. 3. FT-Raman spectra (1064-nm excitation from yttrium-aluminum-garnet-Nd laser, BOMEM DA3 spectrometer) of s-SWNT in  $\text{CS}_2$  solution. The peaks labeled with an asterisk are attributable to  $\text{CS}_2$ .

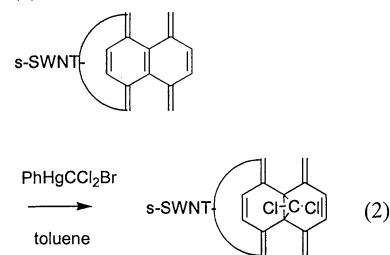
(10, 14, 15), but there is little information on the nature of the nanotubes and the electronic bands that undergo charge transfer. Both iodine and bromine doping completely remove the feature at 0.67 eV in the near-FTIR spectrum of the s-SWNTs (Fig. 4). We conclude that these oxidants completely deplete the first peak in the DOS of the semiconducting SWNT (16). Iodine has a relatively minor effect on the other peaks (due to the first peak in the DOS of the metallic SWNTs), whereas bromine has a stronger effect (the broadened peak shifts to 1.03 eV). We assume that both oxidants remove the electrons from the metallic band, and perhaps also remove some of the electrons from the first peak in the DOS of the metallic SWNTs. The Raman spectrum of iodine-doped s-SWNTs in CS<sub>2</sub> (514.5 nm excitation,  $\omega_r = 171 \text{ cm}^{-1}$ ,  $\omega_t =$

1592 cm<sup>-1</sup>) is similar to that of the pristine s-SWNTs, but the bromine-doped s-SWNTs in CS<sub>2</sub> ( $\omega_r = 251 \text{ cm}^{-1}$ ,  $\omega_t = 1609 \text{ cm}^{-1}$ ) show the expected upshifted radial mode and tangential mode frequencies. The similarity in the Raman spectra of the doped s-SWNTs and doped as-prepared SWNTs (10) suggests that the band gap information obtained from doped s-SWNTs can be used to elucidate the origin of the enhanced conductivity of doped as-prepared SWNTs.

The ultraviolet-visible (UV-vis) spectrum of s-SWNT in CH<sub>2</sub>Cl<sub>2</sub> is featureless, with a shoulder around 250 nm (Fig. 5). Upon doping the s-SWNTs with iodine, new bands appear at 268 nm and 357 nm (control experiments exclude the possibility that these features arise from the pres-

ence of iodine or triiodide anion).

The availability of s-SWNT allows us to explore the chemistry of SWNTs. We chose dichlorocarbene [generated from phenyl(bromodichloromethyl)mercury] because it is an electrophilic reagent that adds to deactivated double bonds (17, 18). Similar reactions have been reported for the fullerenes (19, 20) and for corannulene (21). We recently provided evidence for the functionalization of insoluble SWNT material with dichlorocarbene (4). We exemplify the reaction using our previous notation (4):



A mixture of 16 mg of s-SWNTs and 400 mg of PhCCl<sub>2</sub>HgBr was stirred in 30 ml of toluene at 80°C under argon for 5 hours; 200 mg of PhCCl<sub>2</sub>HgBr was then added and the mixture was stirred at 80°C for another 12 hours. Another batch of 200 mg of PhCCl<sub>2</sub>HgBr was added and the mixture was stirred at 80°C for a further 7 hours. The resulting PhHgBr solid was removed by filtration. The black-colored filtrate was taken to dryness on a rotary evaporator, and the resulting black solid was washed with ethanol and acetone, then dried at room temperature under vacuum to give 5 mg of final product.

Energy-dispersive x-ray spectroscopy showed the presence of ~2 atomic % Cl in the product (these experiments were calibrated with NaCl). The FTIR spectrum shows the C-Cl stretching mode at 798 cm<sup>-1</sup>. The near-IR signal corresponding to the first electronic transition in the semiconducting SWNTs almost disappears, and the signal intensity of the band due to the metallic armchair tubes decreases (Fig. 6). The UV-vis spectrum shows a new absorption band at 297 nm (Fig. 5). The SWNT bands could not be discerned above the strong fluorescence signal in Raman scattering experiments with excitation at 514.5, 647.1, or 1064 nm, which may reflect the change in band structure brought about by the covalent bond formation resulting from addition of dichlorocarbene to the wall of the s-SWNTs. Thus, our results suggest that saturation of ~2% of the carbon atoms in the SWNTs is sufficient to bring about drastic changes in the band electronic structure (22).

We have demonstrated a methodology for preparing solutions of naked carbon metals and semiconductors in organic solutions, and we have shown both ionic (charge transfer) and covalent solution-phase chemistry with concomitant modulation of the SWNT band struc-

**Fig. 4.** Near-FTIR spectra (quartz cell, light path 1/16 inch, Nicolet Magna-IR 560 ESP spectrometer) of s-SWNTs in CS<sub>2</sub> solution (A), iodine-doped s-SWNTs in CS<sub>2</sub> solution (B), and bromine-doped s-SWNTs in CS<sub>2</sub> solution (C). The concentration of s-SWNTs in all solutions was 0.5 mg/ml, and the solvent background was corrected. The solutions were doped to saturation.

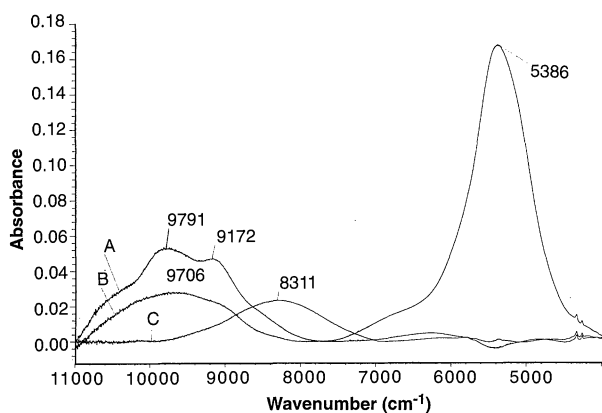


**Fig. 5.** UV-vis spectra (quartz cell, light path 5 mm, Shimadzu UV-2501PC spectrometer) of s-SWNTs in dichloromethane (solid line, solvent-corrected), iodine-doped s-SWNTs in dichloromethane (dashed line, iodine- and solvent-corrected), and dichlorocarbene-functionalized s-SWNTs in dichloromethane (dotted line, solvent-corrected). The concentration of s-SWNTs in all solutions was 0.03 mg/ml.

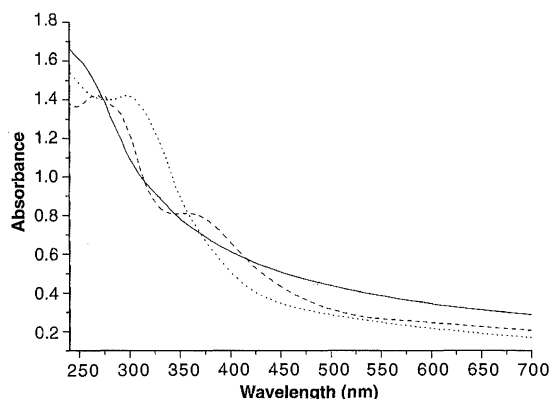
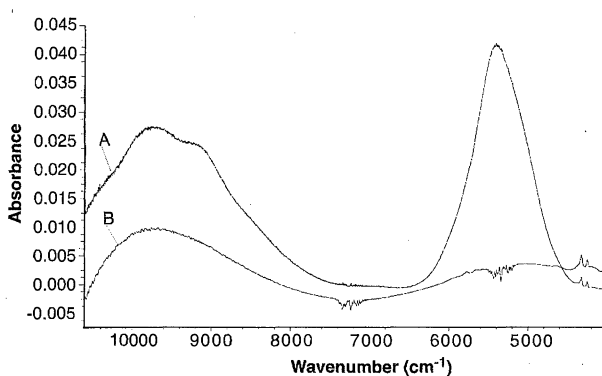


**Fig. 6.** Near-FTIR spectra (quartz cell, light path 1 mm) of s-SWNTs in CS<sub>2</sub> solution (A) and dichlorocarbene-functionalized s-SWNTs in CS<sub>2</sub> solution (B), at the same weight concentration. The s-SWNTs in Figs. 4 and 6 come from different preparations, so the relative ratio of semiconducting chiral tubes and metallic armchair tubes is different.



ture. It is now possible to obtain well-characterized, highly purified SWNT materials that are suitable for physical property measurements. Soluble SWNTs are versatile precursors to copolymer materials with distinctive mechanical and electrical properties and as new ligands for metal complexation.

References and Notes

1. B. I. Yakobson and R. E. Smalley, *Am. Sci.* **85**, 324 (1997).
2. A. Thess *et al.*, *Science* **273**, 483 (1996).
3. C. Journet *et al.*, *Nature* **388**, 756 (1997).
4. Y. Chen *et al.*, *J. Mater. Res.* **13**, 2423 (1998).

5. J. Liu *et al.*, *Science* **280**, 1253 (1998).
6. A. M. Rao *et al.*, *ibid.* **275**, 187 (1997).
7. S. Bandow *et al.*, *Phys. Rev. Lett.* **80**, 3779 (1998).
8. R. C. Haddon, *Nature* **378**, 249 (1995).
9. ———, *ibid.* **388**, 31 (1997).
10. A. M. Rao, P. C. Eklund, S. Bandow, A. Thess, R. E. Smalley, *ibid.*, p. 257.
11. J. W. G. Wildoer, L. C. Venema, A. G. Rinzler, R. E. Smalley, C. Dekker, *ibid.* **391**, 59 (1998).
12. T. W. Odom, J.-L. Huang, P. Kim, C. H. Lieber, *ibid.*, p. 62.
13. T. Pichler *et al.*, *Phys. Rev. Lett.* **80**, 4729 (1998).
14. R. S. Lee, H. J. Kim, J. E. Fischer, A. Thess, R. E. Smalley, *Nature* **388**, 255 (1997).
15. L. Grigorian *et al.*, *Phys. Rev. Lett.* **80**, 5560 (1998).
16. M. S. Dresselhaus, G. Dresselhaus, P. C. Eklund, *Science of Fullerenes and Carbon Nanotubes* (Academic Press, New York, 1996).

17. D. Seyferth, *Acc. Chem. Res.* **5**, 65 (1972).
18. R. C. Haddon, S. V. Chichester, S. M. Stein, J. H. Marshall, A. M. Muijce, *J. Org. Chem.* **52**, 711 (1987).
19. M. Tsuda, T. Ishida, T. Nogami, S. Kurono, M. Ohashi, *Tetrahedron Lett.* **34**, 6911 (1993).
20. J. Osterodt and F. Vogtle, *Chem. Commun.* (1996), p. 547.
21. D. V. Preda and L. T. Scott, *Chem. Eng. News*, 46 (13 April 1998), p. 46.
22. V. H. Crespi, M. L. Cohen, A. Rubio, *Phys. Rev. Lett.* **79**, 2093 (1997).
23. Supported by NSF Experimental Program to Stimulate Competitive Research grant EPS-9452895.

29 July 1998; accepted 31 August 1998

# Ammonia Synthesis at Atmospheric Pressure

George Marnellos and Michael Stoukides

Ammonia was synthesized from its elements at atmospheric pressure in a solid state proton (H<sup>+</sup>)-conducting cell-reactor. Hydrogen was flowing over the anode and was converted into protons that were transported through the solid electrolyte and reached the cathode (palladium) over which nitrogen was passing. At 570°C and atmospheric pressure, greater than 78 percent of the electrochemically supplied hydrogen was converted into ammonia. The thermodynamic requirement for a high-pressure process is eliminated.

The development of a successful process for ammonia synthesis from its elements:



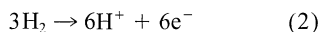
is considered a landmark in heterogeneous catalysis. The Haber process, which involves reaction of gaseous nitrogen and hydrogen on an Fe-based catalyst at high pressures (15 to 30 MPa), was developed at the beginning of the 20th century after an extensive search for an active catalyst (1). Even from early studies, it was realized that the conversion is limited by thermodynamics. The gas volume decreases with reaction; hence, very high pressures must be used to push equilibrium to the right in reaction 1 according to the Le Chatelier principle. The reaction is exothermic (109 kJ/mol at 500°C), and therefore conversion increases with decreasing temperature. However, to achieve industrially acceptable reaction rates, the reaction temperature must be high. The trade-off solution is to operate at temperatures in the range of 430° to 480°C, at which the equilibrium conversion is on the order of 10 to 15% (1).

Despite the very high pressures used and the thermodynamically limited conversion, the Haber process remains after almost a century the dominant route to NH<sub>3</sub> synthesis, a key chemical produced at amounts on the order of 10<sup>8</sup> metric tons per year. We report

on an alternative route to ammonia synthesis at atmospheric pressure through the use of solid state proton (H<sup>+</sup>) conductors by which the requirement for operation at high pressures is eliminated.

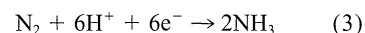
Solid electrolyte cells have been used so far in heterogeneous catalysis to (i) study the mechanism of catalytic reactions (2, 3), (ii) electrochemically alter reaction rates (4, 5), and (iii) cogenerate electricity and useful chemicals (6). The solid electrolytes used in most of the above applications were oxygen ion conductors. In the last decade, however, materials that exhibit protonic conductivity in the solid state have been introduced into catalysis research (7). These H<sup>+</sup> conductors are particularly useful because they can operate at temperatures in which many industrial hydro- and dehydrogenation reactions take place. Furthermore, in contrast to oxidation reactions, a number of industrial hydrogenations (ammonia and methanol production) are equilibrium limited at the operating conditions.

A model process that uses solid state proton conductors to obtain conversions higher than those predicted by the reaction equilibrium has previously been proposed (8). The principle is as follows. Gaseous H<sub>2</sub> passing over the anode of the proton-conducting cell-reactor, will be converted to H<sup>+</sup>:



The protons (H<sup>+</sup>) are transported through the solid electrolyte to the cathode where the

half-cell reaction



takes place. Thus, reaction 1 is again the overall reaction. We have verified experimentally the above model process and present the results here.

A schematic diagram of the cell-reactor we used is shown in Fig. 1. It consisted of a nonporous ceramic tube (18 cm long, 1.25-cm inside diameter and 1.55-cm outside diameter) closed at the bottom end. The ceramic material was a strontia-ceria-ytterbia (SCY) perovskite of the form SrCe<sub>0.95</sub>Yb<sub>0.05</sub>O<sub>3</sub>. This solid has good mechanical strength and high protonic conductivity (9). The ceramic tube was enclosed in a quartz tube (20 cm long, 3.60-cm inside diameter, and 4.10-cm outside diameter). Two porous polycrystalline palladium films were deposited on the inside and outside walls of the SCY tube and served as cathodic and anodic electrodes, respectively (Fig. 1). The solid state device constructed can be represented by the cell H<sub>2</sub>, Pd | SCY | Pd, N<sub>2</sub>, NH<sub>3</sub>, He.

The electrode preparation and characterization procedure has been described in detail elsewhere (10). The superficial surface area of each electrode was 1.3 cm<sup>2</sup>, and the true

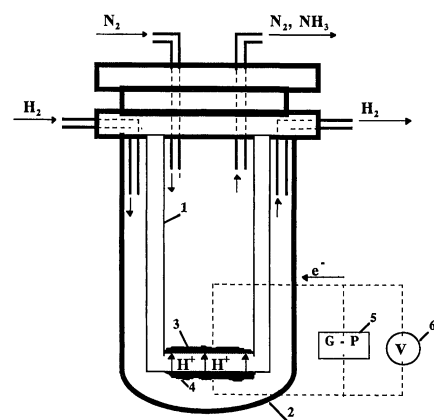


Fig. 1. Schematic diagram of the cell-reactor: 1, SCY ceramic tube (H<sup>+</sup> conductor); 2, quartz tube; 3, cathodic electrode (Pd); 4, anodic electrode (Pd); 5, galvanostat-potentiostat; and 6, voltmeter.

Chemical Engineering Department and Chemical Process Engineering Research Institute, Aristotle University of Thessaloniki, Thessaloniki 54006, Greece.